J Petrol Explor Prod Technol (2017) 7:265–279
DOI 10.1007/s13202-016-0260-8

ORIGINAL PAPER - PRODUCTION ENGINEERING

Examination of unconventional phenomena in naturally fractured liquid-rich gas reservoirs: single-block compositional model

B. N. Al Ghamdi[1] · L. F. Ayala H.[1]

Received: 12 January 2016 / Accepted: 22 May 2016 / Published online: 7 June 2016

Abstract During the depletion of liquid-rich gas reservoirs, the gas condenses as the pressure inside the reservoir reduces below the hydrocarbon dew-point pressure, which introduces retrograde condensate. In such conditions, the productivity experiences a reduction in recovery due to the appearance of condensate near the production channels. This work is aimed to provide insight on productivity characteristics of a liquid-rich gas system in unconventional environments and extend the scrutiny on the propagation of condensate while activating capillary forces and diffusion. The impact of capillary pressure on phase behavior was explored using an in-house generated coupled phase behavior model with a capillary pressure equation. The influence of capillary pressure was examined against different sets of composition combinations in different reservoir settings. Capillary force extents were highly dependent on composition combinations and pore throat radiuses. Mixtures with higher volatile concentrations showed the highest capillary forces. The enhancement in condensate propagation, resistance to gas flow, and impact on recovery were explored at 10- and 20-nm pore throat sizes. The investigation suggested that interfacial tensions implied greater influence on the flow behavior in oil-dominated systems than in gas-dominated conditions. Evaluating the flow performance of unconventional phenomena in liquid-rich gas reservoirs was extended to include diffusion while activating capillary forces. The results showed higher domination of diffusion on reservoir performance, which provided additional fluid recovery. Subsequently, the enhanced withdrawal of fluid dismissed the impact of capillary forces on gas flow and the impact of condensate blockage.

Keywords Liquid-rich gas reservoirs · Naturally fractured systems · Condensate blockage · Capillary pressure · Diffusion

List of symbols

c_i	Overall molar composition of the ith component
f_{gi}	Fugacity of the ith component in vapor phase
f_{li}	Fugacity of the ith component in liquid phase
f_{ci_g}	Fugacity of the mixture as a function of vapor-phase pressure
f_{ci_o}	Fugacity of the mixture as a function of liquid-phase pressure
K_i	Vapor–liquid equilibrium ratio of the ith component
MW_g	Molecular weight of gas (lb/lbmol)
MW_o	Molecular weight of oil (lb/lbmol)
p_g	Pressure of the gas phase (psia)
p_o	Pressure of the condensate phase (psia)
Pn_i	Parachor coefficient of the ith component (unitless)
r	Pore throat radius (nm)
x_i'	Normalized second-phase liquid mole fractions of the ith component
X_i	Second-phase liquid mole number of the ith component
x_i	Molar composition of the ith component in the condensate phase

✉ B. N. Al Ghamdi
bander_nasser@hotmail.com; bna111@psu.edu

L. F. Ayala H.
ayala@psu.edu

[1] John and Willie Leone Family Department of Energy and Mineral Engineering, EMS Energy Institute, The Pennsylvania State University, University Park, PA 16802, USA

y'_i Normalized second-phase vapor mole fractions of the ith component
Y_i Second-phase vapor mole number of the ith component
y_i Molar composition of the ith component in the gas phase

Greek

ϕ_{ci} Fugacity coefficient of the ith component in the mixture
ϕ_{gi} Fugacity coefficient of the ith component in vapor phase
ϕ_{li} Fugacity coefficient of the ith component in liquid phase
ρ_g Specific gas density (lbm/ft^3)
ρ_o Specific oil density (lbm/ft^3)
σ Interfacial tension (dyne/cm)

Introduction

Liquid-rich gas reservoirs are abundant in condensate content despite its classification as gas reservoirs. Undersaturated liquid-rich gas reservoirs are presented initially in a gaseous phase. Once depletion is undertaken and the pressure drops below dew point, condensate will drop out and accumulate near the production channels. The accumulation period is relevant to the fluid's characteristics and depends on the production settings. During the accumulation period, the productivity declines due to the impairment of flow near the flowing channels. The severity of such experience becomes significant in tighter formations. According to Ayyalasomayajula et al. (2003), this phenomenon may cost loses to the production by 40–80 % of its estimates while flowing in a single phase.

The complexity of producing from gas reservoirs is associated with the intricate properties of the fluid and the flow mechanism in heterogeneous reservoirs with strongly varying rock properties. The connectivity of the pore space, known as permeability, allows the fluids to travel according to the drive mechanism. Low permeability is associated with poor connectivity between the pores and subsequently leads to poor flow performance. Gas formations with permeability less than 1 mD are defined as tight reservoirs, while formations with permeability less than 0.001 mD are referred to as ultra-tight reservoirs (Abaa et al. 2012). Considering the flow phenomenon of liquid-rich gas reservoirs, tight and ultra-tight formations can be a very complex hosting environment to achieve economical production.

Holditch (2006) mentioned that the definition of tight reservoirs is not limited to permeability but includes other physical factors. Fluids flowing under Darcian law depend on permeability, viscosity, and the pressure gradient. Darcy's law dominates the flow regime in porous media under isothermal conditions as long as the flow is continuous and laminar. In the case where the flow of fluids in the reservoir becomes impaired due to formation tightness or resistance by other fluids, such as with condensate buildup, Fick's law prevails. Fick (1855) introduced the idea of the exchange of matters through a porous media by diffusion, where the molecules are exchanged at random motions. His law applies when there is a molecular to molecular interaction, or molecular to surface interaction. The flow of fluid in this case is a function of the diffusion coefficient and the concentration gradient. Ertekin et al. (1986) introduced the concept of multi-mechanistic flow, where the flow of fluids submits to Darcian and Fickian law. In tight reservoirs with low permeable flow paths, the gas flows in the pressure domain under Darcy's law and flows by diffusion in concentration domains under Fick's law.

The multi-mechanistic flow concept was adopted in the work of Ayala et al. (2004, 2006, 2007) to assess the impact of multi-mechanistic flow on naturally fractured retrograde gas reservoirs using a compositional model. A reservoir depicting the concept of a "sugar cube" initiated by Warren and Root (1963) was considered with the fractured permeability being the highest, while assuming constant diffusion coefficients throughout the simulation period. The study evaluated the recovery of gas condensate in tight formations with permeability ranging from 1 to 0.0001 mD, and the consideration of different diffusion coefficients. It was concluded that the permeability of the reservoir is the controlling factor of the flow mechanism in tight formations. Fickian flow was responsible for the flow of fluids through the reservoir when the permeability of the matrix was less than 0.001 mD, while Darcian flow was dominant when the permeability was 0.1 mD and more. At the conditions where Darcian and Fickian laws were both responsible for the flow, ultimate recovery reached up to four times larger than the recovery when the flow was obeying Darcian law alone. However, capillary forces were neglected throughout the research, which could have contributed an additional constraint against the movement of the gas.

Fluids are highly dependent on the transport properties and the capillary forces between the fluids-in-place and the rock itself (Phillip et al. 2010). As a result, permeability, relative permeability, and wettability conditions are highly influential on the flow mechanism, whereas capillary pressure is a function of saturation and it controls the distribution of fluids in the pore spaces. It occurs as a function of the interfacial tensions (IFTs) between the wetting and non-wetting phase, and the characteristics of the hosting rock (Ahmed 2000).

The relationship between surface tension and the physical properties of fluids-in-place was pioneered by Ramsay and Shields (1893), Macleod (1923), Sugden (1924) and Ellis (1932). As temperature increases, liquid density decreases, and subsequently, surface tension decreases. The findings came in accordance with the assumptions of Van der Waals (1910) on the fundamental relationship between cohesion forces and density, where the distance between molecules controls the attraction forces. Thus, as temperature increases, the attraction between molecules decreases causing a split in phases. Macleod (1923) and Sugden (1924) introduced an empirical equation relating density and surface tension of pure substance. The equation was presented as a function of the difference in molar densities and surface tension. Higher changes in IFT were associated with higher liquid density. Weinaug and Katz (1943) extended the work of Macleod and Sugden and developed an expression that is applicable for mixtures based on the same fundamentals.

Nojabaei et al. (2013) investigated the effect of capillary pressure on the behavior of oil reservoirs in tight rocks utilizing the Macleod and Sugden equation. The author has concluded that for oil reservoirs, there is an inverse relationship between capillary pressure and bubble-point pressure. It was found that capillary pressure increases with smaller pore throat sizes and bubble-point pressure appeared to be decreasing with smaller pore throat sizes. These outcomes were implied in later research conducted by Nojabaei et al. (2014) to investigate the influence on the productivity of Bakken oil reservoir in an oil-wetting environment. Contrary to the common belief of oil-wet systems implying higher retention and intensive holding of oil-in-place, the results showed an increase in oil recovery by 7–9 and 10 % in the gas recovery.

The study is aimed to demonstrate the impact of capillary forces on the phase behavior of liquid-rich gas reservoirs while implying higher retention of oil inside the nanopores of the formation. Great emphasis will be regarded toward capturing the influence of capillary pressure on phase behavior, dew-point pressure, residence of condensate, and resistance against gas flow. Furthermore, this research is expected to map the significance of including diffusion while activating capillary forces on the flow performance of liquid-rich gas reservoirs in tight settings surrounded by fractures.

Coupling a phase behavior model with a capillary pressure equation

Fluid behavior inside reservoirs is captured through the use of an equation of state (EOS) as part of a phase behavior model (PBM), which traditionally conducts flash calculations at a given pressure, overall composition, and temperature. In this research, the PBM is improved to capture changes in the reservoir as a function of the pore throat radius. In the absence of capillary pressure with the traditional PBM, the pressure is the same for both phases, and the fluid properties are calculated as a function of the same pressure. With the inclusion of capillary pressure, the vapor–liquid equilibrium flash needs to be adjusted to accommodate for calculating the fluid properties of each phase according to the phase pressure. The simulator requires the pressure of the dominant phase, and through capillary pressure, the pressure of the second phase is estimated. The determination of capillary pressure is embedded with the determination of IFT, and both are function of the pore throat size and the physical properties of the phases. Capturing the physical properties of the mixture comes as a result of quantifying the fraction of each phase, and phase preference inside the pores. Fluid properties become known once the reservoir is at thermodynamic equilibrium, which is achieved once a potential transfer of a component between the two phases is halted. After each thermodynamic equilibrium convergence, the developed model examines the stability conditions of the mixture. The goal is to find the maximum capillary pressure as a function of the IFT properties found at dew-point pressure given pore radius. Once the dew-point is found, IFT is calculated using molecular weights and densities of the phases. The final step is to calculate capillary pressure as a function of IFT and radius of the pores and then to conduct an equality check on capillary pressure and IFT using an iterative technique.

First, in order to examine the stability of the fluid-in-place under two-phase pressures, the Michelsen (1982) method is modified while creating the second phase inside the mixture. All of the steps in the fugacity calculations consider the selection of the Z-factor root that minimizes Gibbs free energy. Vapor-like second mixture calculations are initiated by calculating the mixture fugacity (f_{ci_o}) as a function of the liquid-phase pressure and overall composition (c_i) as shown in Eq. (1).

$$f_{ci\_o} = \phi_{ci} \cdot c_i \cdot p_o; \quad i = 1, 2, \ldots n_c \tag{1}$$

$$\phi_{ci} = f(c_i \cdot p_o) \tag{2}$$

Then, the vapor second-phase fugacity (f_{gi}) is measured using vapor-phase pressure and the normalized second-phase vapor mole fractions (y'_i), which can be calculated using Eq. (3).

$$f_{gi} = \phi_{gi} \cdot y'_i \cdot p_g; \quad i = 1, 2, \ldots n_c \tag{3}$$

$$y'_i = \frac{c_i \cdot K_i}{\sum_i^{n_c} (c_i \cdot K_i)} \tag{4}$$

Liquid-like second mixture calculations are initiated by calculating the mixture fugacity (f_{ci_g}) as a function of the

vapor-phase pressure and overall composition (c_i) as shown below.

$$f_{ci\_g} = \phi_{ci} \cdot c_i \cdot p_g; \quad i = 1, 2, \ldots n_c \tag{5}$$

$$\phi_{ci} = f(c_i \cdot p_g) \tag{6}$$

Afterword, the liquid second-phase fugacity (f_{li}) is measured using liquid-phase pressure and the normalized second-phase liquid mole fractions (x'_i), as illustrated below.

$$f_{li} = \phi_{li} \cdot x'_i \cdot p_o; \quad i = 1, 2, \ldots n_c \tag{7}$$

$$x'_i = \frac{(c_i/K_i)}{\sum_i^{n_c} (c_i/K_i)} \tag{8}$$

Once fugacities of the mixture and second phase are measured, the K-values are updated until convergence or trivial solution is achieved. Updating K-values is conducted for each of the created phases separately by checking for the conditions described by Eqs. (9) and (10).

$$\text{Convergence criterion: } \sum_i^{n_c} (R_i - 1)^2 < 10^{-10}; \quad i = 1, 2, \ldots n_c \tag{9}$$

$$\text{Trivial solution criterion: } \sum_i^{n_c} (\text{In}K_i)^2 < 10^{-4}; \quad i = 1, 2, \ldots n_c \tag{10}$$

where:

$$R_i = \frac{f_{ci\_o}}{f_{gi}} \frac{1}{\sum_i^{n_c} (c_i \cdot K_i)}; \quad \text{for vapor second-phase} \tag{11}$$

$$R_i = \frac{f_{li}}{f_{ci\_g}} \sum_i^{n_c} (c_i/K_i); \quad \text{for liquid second-phase} \tag{12}$$

$$K_i^{(n+1)} = K_i^{(n)} \cdot R_i \tag{13}$$

$$S_V = \sum_i^{n_c} (c_i \cdot K_i) \tag{14}$$

$$S_L = \sum_i^{n_c} (c_i/K_i) \tag{15}$$

Once a solution has been achieved for both cases, the mixture is determined to be in two phases if either of the tests revealed $S > 1$. In contrast, the mixture is in a single phase if both tests arrive at a trivial solution, both tests produce $S \leq 1$, or one of the tests yields trivial solution and the other one gives $S \leq 1$.

Second, the phase equilibrium model is modified to predict the compositional behavior of a fluid system as a function of two-phase pressure, composition, and temperature. In conditions where single phase prevails, phase behavior model will utilize the initial phase pressure. However, under two-phase conditions, the fugacity of a component in liquid phase (f_{li}) is calculated as a function of liquid-phase pressure and is compared to the fugacity of the gaseous phase (f_{gi}) calculated as a function of vapor-phase pressure. Equations (16) and (17) are used to attain fugacities and update K-values through the successive substitution method (SSM) until a net transfer of zero is achieved.

$$f_{gi} = \phi_{gi} \cdot y_i \cdot p_g; \quad i = 1, 2, \ldots n_c \tag{16}$$

$$f_{li} = \phi_{li} \cdot x_i \cdot p_o; \quad i = 1, 2, \ldots n_c \tag{17}$$

where:

$$\phi_{gi} = f(y_i \cdot p_g) \tag{18}$$

$$\phi_{li} = f(x_i \cdot p_o) \tag{19}$$

$$K_i^{(n+1)} = K_i^{(n)} \cdot \left(\frac{f_{li}}{f_{gi}}\right)^{(n)} \tag{20}$$

$$\text{Convergence criterion: } \sum_i^{n_c} \left(\frac{f_{li}}{f_{gi}} - 1\right)^2 < 10^{-13} \tag{21}$$

After a thermodynamic equilibrium is reached, the composition of all the phases can be reliably estimated using the recent K-values. Furthermore, the properties of vapor and liquid can be predicted easily using the pressure of each phase accordingly and can include the estimation of molecular weights, densities, and viscosities. Weinaug and Katz (1943) developed an expression as illustrated in Eq. (22), which is implemented to estimate IFT and capillary pressure once the physical properties are obtained. The determination of capillary pressure is implicit; it depends on the changes in IFT, radius of the pores, and thermodynamic changes.

$$\sigma = \sum_i^{n_c} \left[P_{n_i} \left(x_i \frac{\rho_o}{MW_o} - y_i \frac{\rho_g}{MW_g} \right) \right]^4 \tag{22}$$

$$P_c = \frac{2\sigma}{r} \tag{23}$$

The validity of the developed modified Michelsen (1982) method and the phase behavior model was examined by reproducing similar results to those generated by Nojabaei et al. (2013). Although their work was concentrated on bubble point and oil reservoirs, there was little emphasis on the liquid retrograde region. The goal of this paper is to demonstrate the influence of capillary forces on the upper dew-point curve of liquid-rich gas reservoirs.

Examining capillary pressure in nanopores under different conditions

Capillary pressure exists with the presence of two immiscible fluids in contact with each other through an interface. The curvature of the interface represents the difference in pressure between the two fluids. Once condensate appears in the system under dew-point pressure, it will start to compete with the gas for flow paths. The magnitude of impairment is determined by the composition concentrations. Mixtures with higher non-volatile concentrations will form thicker condensate coating and impose greater impairment (Al Ghamdi 2009). The hypothesis in this research suggests that capillary pressure would increase the residence time of condensate and impose higher resistance impacting productivity. In this work, the effect of capillary pressure with the inclusion of different composition combinations is examined to capture the influence on dew-point pressure of liquid-rich gas systems.

Capillary pressure causes different effects on saturation pressure based on the compositions of the fluids-in-place. Several combinations including methane—butane, methane—hexane, and methane—decane were used for the analysis. The three binary mixtures selected are meant to represent light, moderate, and heavy mixtures. The same concentration combinations were used for the three mixtures, where the non-volatile component increases from 15 to 40 %. As the non-volatile concentration increases, the mixture becomes richer in heavies and the phase envelope shifts to the right toward higher temperatures. Similar testing was conducted on various pore throat sizes to capture changes in capillary pressure, interfacial tension, and dew-point pressure.

Figure 1 shows capillary pressure for the different combinations versus pore throat sizes. As the pore radius becomes smaller, capillary pressure increases for most of the combinations tested. Despite expecting methane–decane to exert the highest capillary pressure, methane—hexane and methane–butane showed the highest values with concentrations of 85 and 15 %, respectively. The rest of the combinations were compiled between capillary pressures of 0 and 5 psia. Mixtures with higher non-volatile concentrations deliver more condensate than those with the least heavies. As the condensate phase becomes dominant inside the pores, the capillary pressure moves toward zero. Thus, the light and moderate mixtures reflected the highest capillary pressures.

Figure 2 reflects the interfacial tension against various nanopores. Higher changes in capillary pressure are associated with higher changes in interfacial tensions. The moderate and lightest mixtures continue to show the highest interfacial tension as seen with the capillary pressure. Interfacial tension for all the cases decreases as the pore throat sizes shrink, but with noticeable differences between the mixtures recording the highest IFT and the rest of the binary mixtures. The reason the two mixtures mentioned standout is due to the differences in the phase densities as shown in Fig. 3. Larger differences in phase densities reflect higher IFT and capillary pressure according to Eqs. (22) and (23). In addition, Fig. 3 illustrates the magnitude of divergence between the three binary mixtures indicating lower IFT values for methane–decane even at higher temperatures.

Mixtures with higher capillary pressure and IFT reflect a notable increase in the upper dew-point pressure. Methane–butane and methane—hexane with 85 % volatile and 15 % non-volatile concentration continued to show the highest impact on the upper dew-point curve. Figure 4 illustrates the influence of capillary pressure on dew-point pressure as the pore throat size becomes smaller. These values were generated at a fixed temperature. The plot demonstrates the magnitude of change in dew-point pressure after activating capillary pressure in contrast to the case where the dependency on the character of the rock is neglected.

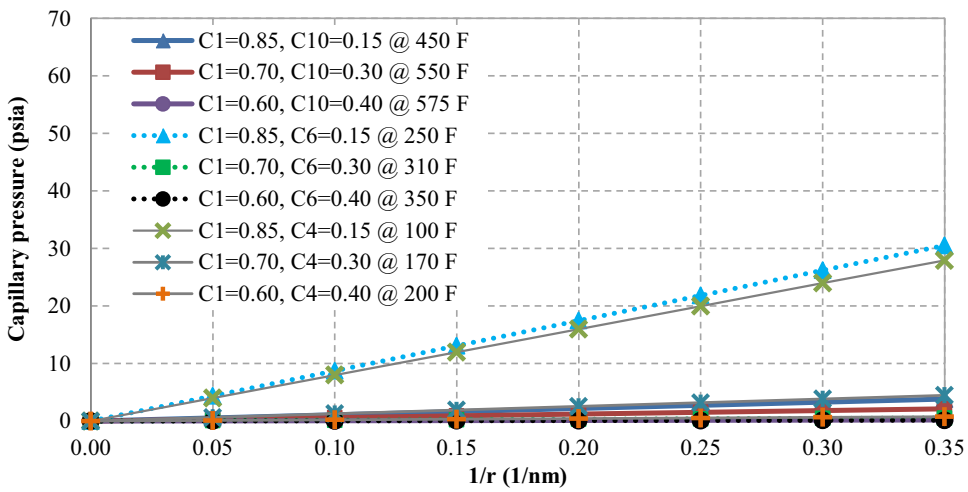

Fig. 1 Capillary pressure for binary mixtures with different concentrations

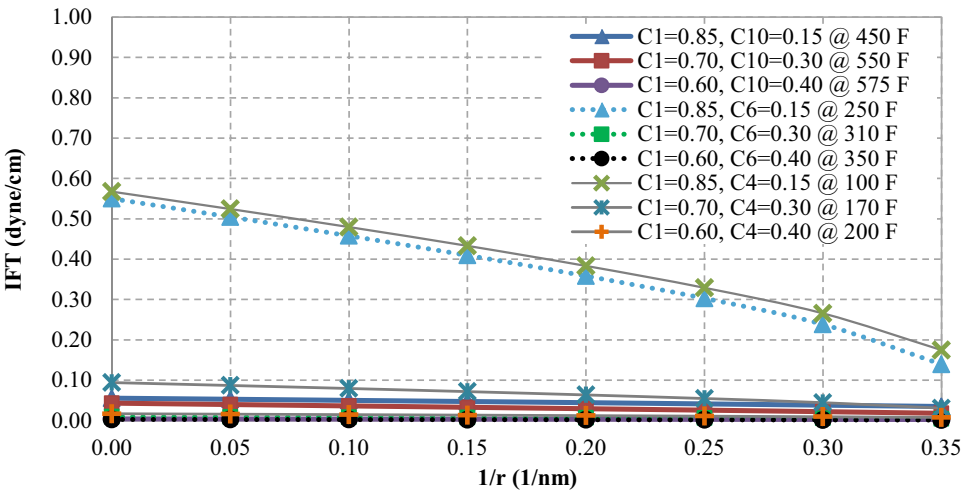

Fig. 2 Interfacial tension for binary mixtures with different concentrations

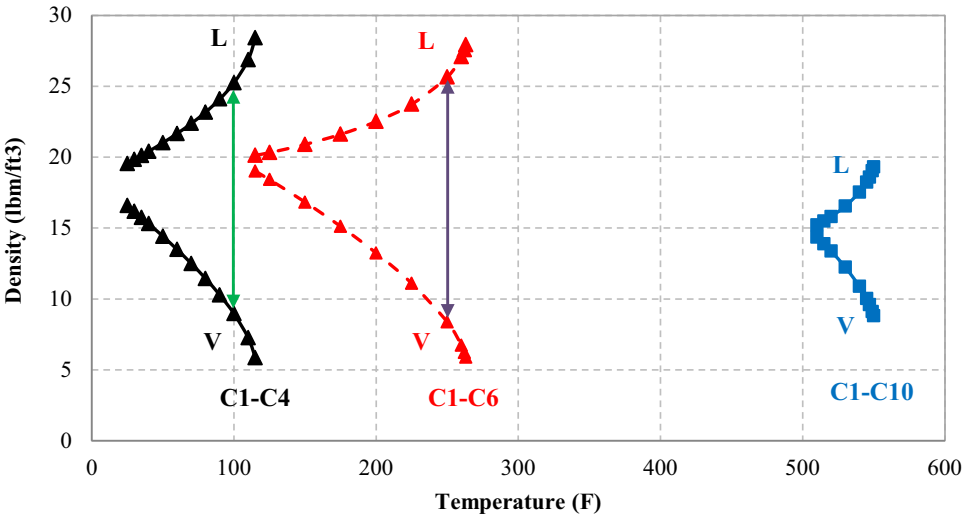

Fig. 3 Vapor and liquid densities versus temperature for different mixtures

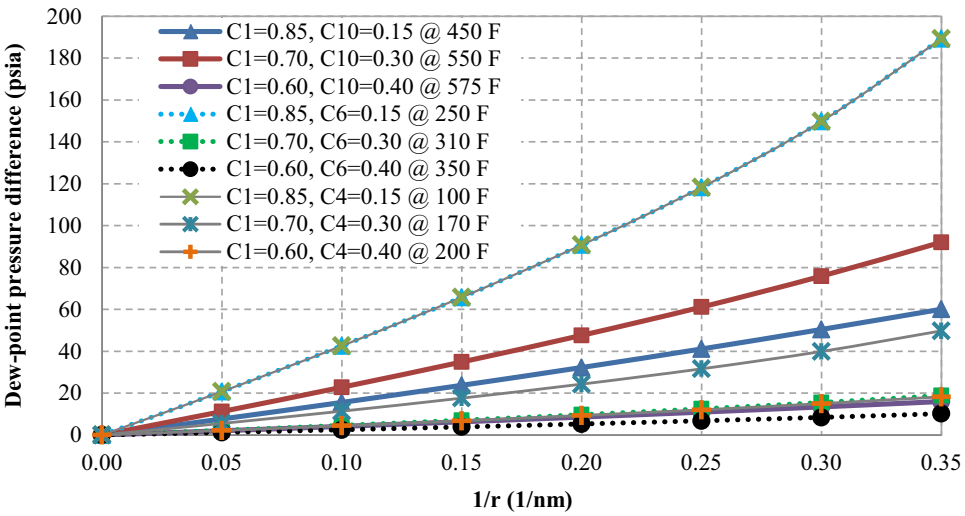

Fig. 4 Dew-point pressure difference for mixtures with different concentrations

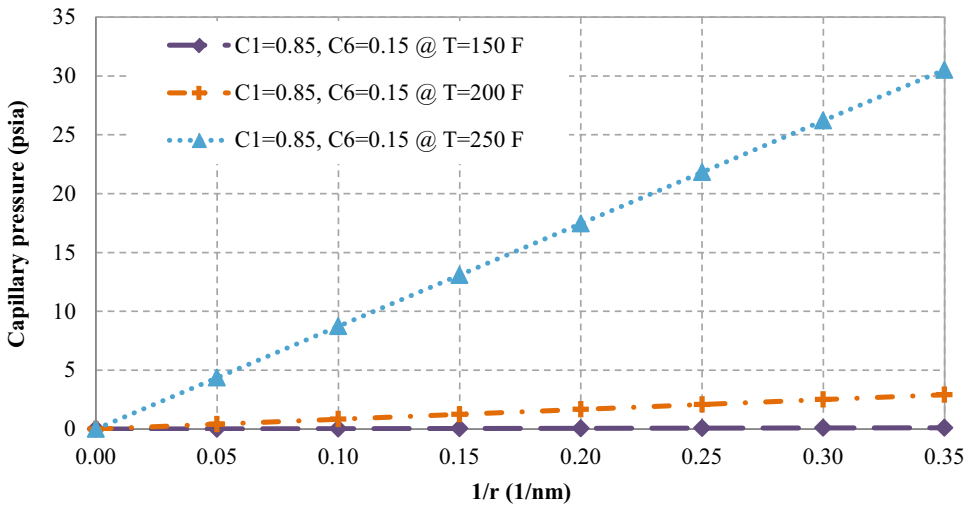

Fig. 5 Capillary pressure for methane–hexane at different temperatures

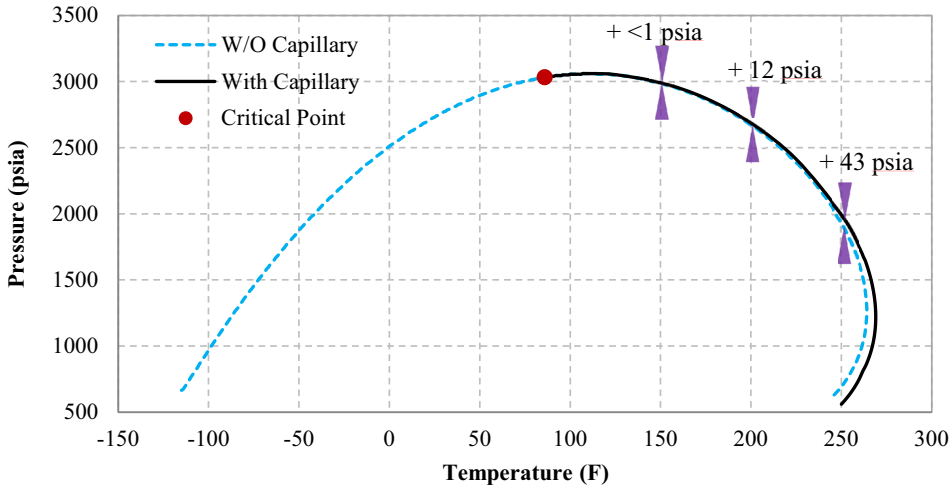

Fig. 6 Influence of capillary pressure on the phase envelope of methane–hexane (85–15 %)

Methane—hexane reflects higher capillary pressure, IFT, and influence on dew-point pressure as long as the mixture is rich in volatile concentration. The same applies to methane–butane with 85 and 15 % composition. Although the mixture of methane–butane with 70 and 30 % shows higher capillary pressure and IFT than the rest of the mixtures, it does not return higher influence on dew-point pressure. In comparison, methane–decane with ≥70 % methane reflects higher influence on dew-point pressure than methane–butane with 70 % methane concentration. This contrast is owed to one mixture being lean and the other being richer in heavies.

Investigating the influence of temperature revealed greater impact of temperature on capillary pressure and subsequently dew-point pressure. Capillary pressure behavior versus decreasing pore throat radius was explored at increasing temperatures using methane–hexane (85–15 %). The outcome demonstrated in Fig. 5 shows that closer to a critical point, IFT values reach zero, where neither capillary pressure nor dew-point pressure changes occur. As the temperature increases, higher capillary pressure is attained due to having less oil toward the cricondentherm. In general, the highest capillary pressure is found at the lowest oil saturation. The influence of capillary pressure on increasing temperature at the upper dew-point pressure is illustrated by Fig. 6, where the increase ranges between <1 and 200 psia.

The influence of capillary pressure on near critical fluids

Several mixtures with various compositional combinations have been used to apply different severities of condensate coating. Each case was simulated for a period of 1000 days, with and without the activation of capillary pressure. These runs were associated with various condensate contents, which presumably imply different

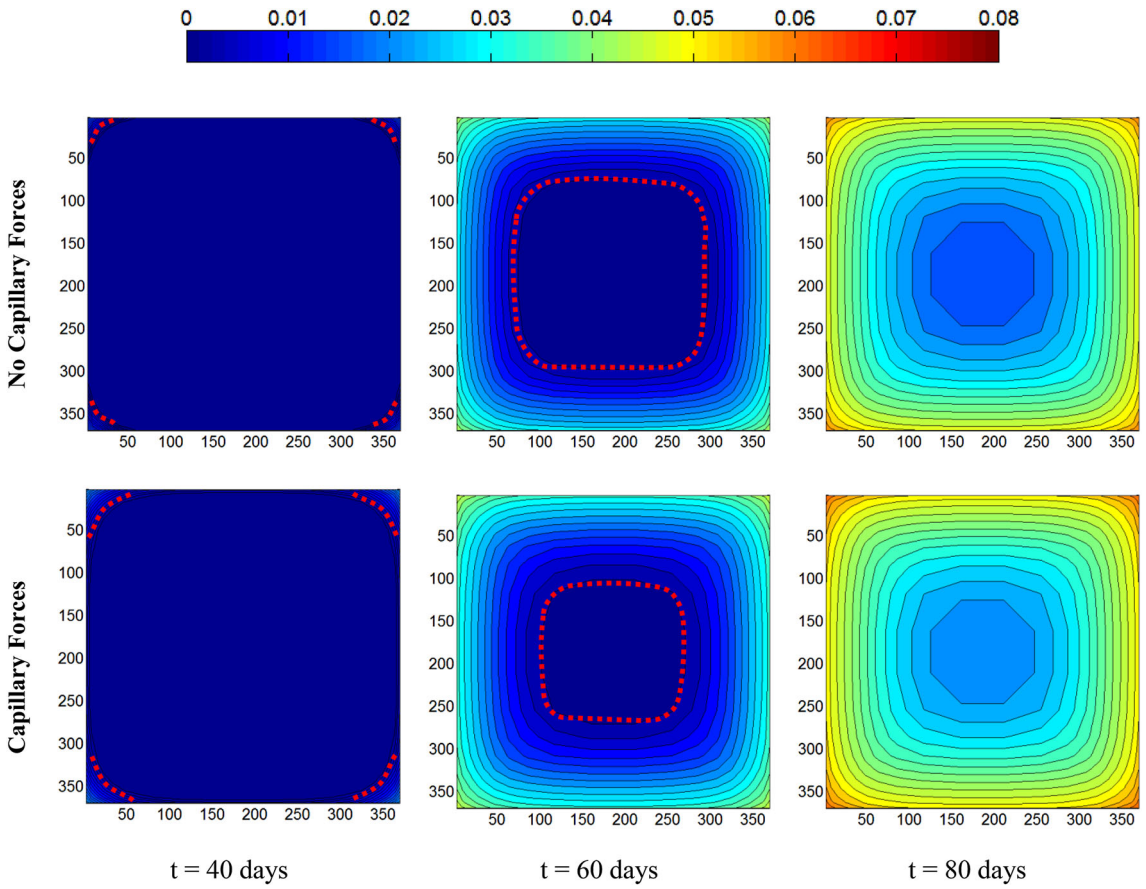

Fig. 7 Condensate evolution for methane–hexane (85–15 %) with the inclusion of capillary forces ($r = 10$ nm)

blockage once capillary forces are activated. For each binary mixture, a temperature was chosen for the testing that is located halfway between the critical point and the cricondentherm temperature. The selection of the temperature at the specified location was aimed to promote condensate recovery at separator conditions. A developed in-house compositional simulator was used for the analysis with a reservoir grid system consisting of 22 × 22 × 1 blocks and surrounded by fractures. The governing equations of the simulator are introduced in "Appendix 2." The concept of a single-matrix block is utilized in this research as an elemental volume where fluids are accumulating and flowing into and out of the system. Fractures were placed surrounding the system from the sides, and all the sides of the block are open for flow upon the establishment of boundary conditions. The fractures impose the flow path with higher permeability, while the matrix is presented with the least permeability and stores most of the fluids-in-place. In the selection of the grid block sizes, refined blocks with the size of 5 ft were assigned to the neighboring blocks of the fractures to capture detailed performance of condensate evolution. The blocks that are in the center of the single-block configuration have the largest size, not exceeding 50 ft, while the blocks in between range in size from 7.5 to 37.5 ft, in increasing order toward the inner portion of the matrix system. Selecting the length and number of blocks was achieved with care after considering discretization analysis and computational capabilities. With a quarter-block representation, a grid system of 11 × 11 × 1 can reproduce the same results of a single block after multiplying the output by 4. Tables 1 and 2 in "Appendix 1" show the data used as parameters for the simulation study.

A methane–hexane mixture with concentration of 85 and 15 % was used for the analysis since it reflected the highest capillary forces. This moderate mixture was used to assess condensate evolution in a reservoir with a pore throat radius of 10 nm. Figure 7 illustrates the influence of activating capillary forces against a base case where no capillary forces were used. The evolution of condensate is captured through monitoring condensate saturation progress against time using aerial view maps. Since the dew point is higher with capillary forces, condensate is expected to appear earlier. For this mixture with 85 and 15 % concentration, the liquid dropped out 3 days earlier than before, which covered 3 % of the number of blocks by the

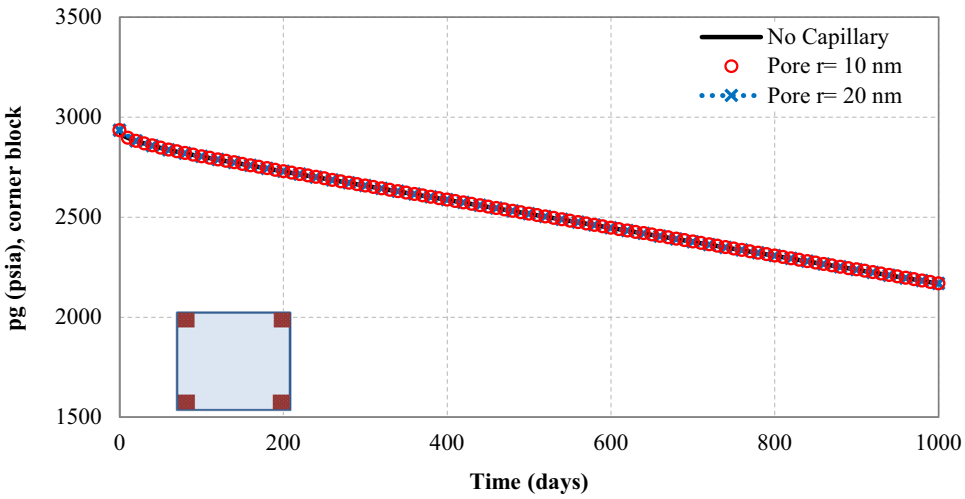

Fig. 8 Reservoir pressure for methane–hexane at the corners of the single block with different pore throat sizes

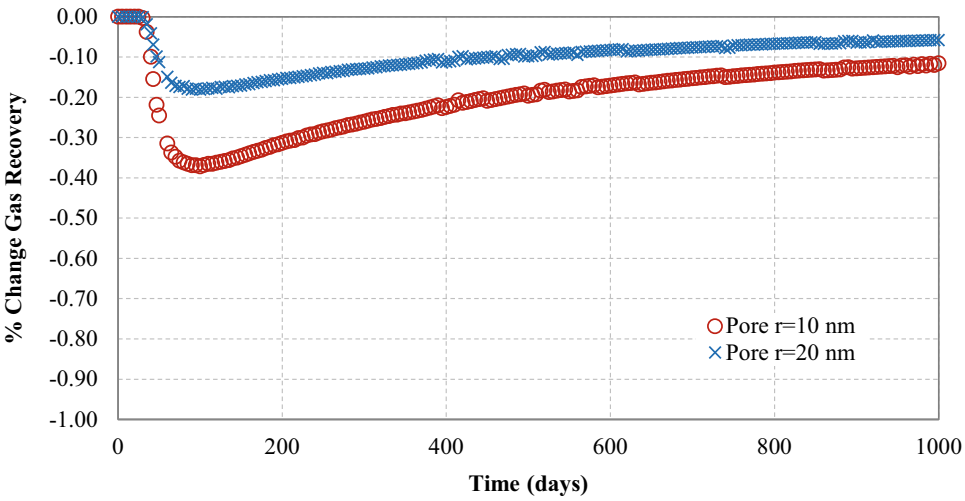

Fig. 9 Percent change in gas recovery for methane–hexane (85–15 %)

end of 30 days. After 40 days, condensate had appeared in 44 % of the blocks in comparison with 23 % without activating capillary pressure. This indicates that capillary pressure had increased the spread of condensate by 91.3 % at the specified time. As time progressed and condensate reached the inner part of the block, the increase in spread became smaller. After 60 days of simulation, more than 93 % of the blocks had accumulated some condensate, which is only a 5 % increase from the case without capillary pressure. Although the spread was enhanced, the values of saturation were still low.

Figure 8 shows the reservoir pressure profile of the moderate mixture captured at the corners of the matrix system. It compares the pressure profile while activating capillary forces using a pore throat radius of 20 and 10 nm to the case that neglected capillary effects. As shown from the plot, the depletion behavior of the reservoir was mirrored under the conditions specified. The outcome indicated minuscule effects of capillary forces on reservoir pressure. Furthermore, insignificant influence was noted with the oil saturation profile. In fact, all the case studies showed similar behavior suggesting restricted influence of capillary forces on reservoir pressure and oil saturation.

It is essential to evaluate the impact on recovery in order to understand the contribution of the matrix to production in nanopores, knowing that capillary forces will employ retention on the movement of fluids. Recovery behavior in liquid-rich gas systems reflects similar surface molar, gas, and condensate recovery until the pressure drops below dew point and condensate appears in the reservoir. Once condensate starts to accumulate in the system, the recovery profile of the molar recovery and condensate recovery depart from the recovery of the gas.

As seen earlier, capillary pressure applied diminutive influences to increase the residence time of condensate, which is expected to impose resistance of the same power to impact productivity. For a better demonstration, instead of illustrating overlapping curves that have little difference to display, percent change was calculated in reference to the results that rendered the capillary forces null. Figures 9 and

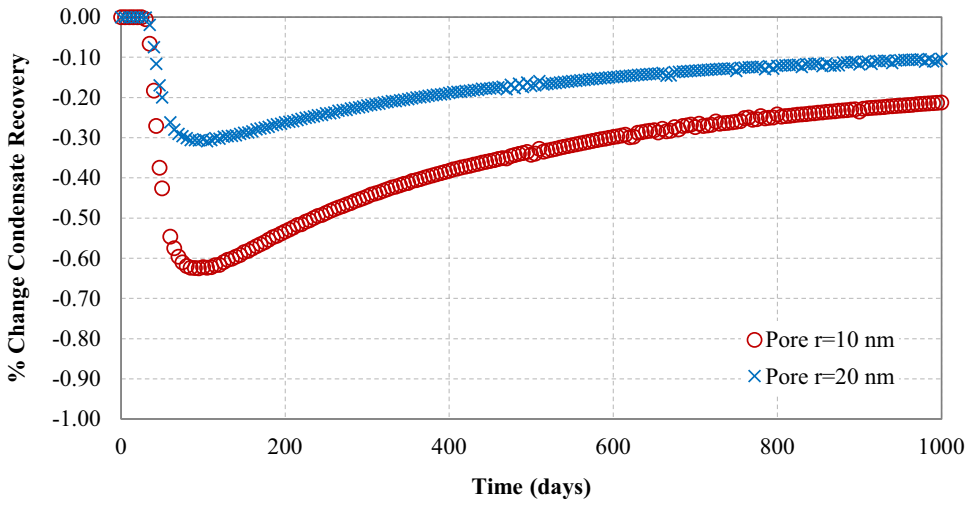

Fig. 10 Percent change in condensate recovery for methane–hexane (85–15 %)

10 display percent change in gas and condensate recoveries using the positive–negative scale to indicate the influence of capillary pressure in nanopores. Eventually, both plots show decreases in recoveries, and the most significant loss is seen with the smallest pore throat radius. Although the reduction in recoveries does not exceed 1 %, it is seen as an impact within the limited scale of influence that has been witnessed. The highest magnitude in reduction is linked to the period when condensate spread was enhanced, which took place in the first 120 days. Eventually, gas recovery was reduced due to the increase in flow resistance. The reduction in condensate recovery is owed to losing condensate to the formation, resulting from the elongated residence time of condensate. The question that remains to be answered: why is there a less evident impact on the performance of liquid-rich gas reservoirs in contrast to the impact on oil reservoirs seen in the work of Nojabaei et al. (2013)?

Interfacial tension based on fluid-dominant system

Near the critical point, where the bubble-point curve and dew-point curve interconnect, the physical properties of the liquid and gas are indistinguishable. Due to the similarity in the properties, the differences in densities are minimal, which produce zero IFT values. Away from the critical point, where the physical properties of the two phases are apart from each other, IFT values vary in magnitude. Capillary pressure and IFT have the highest values at the initial contact between the two immiscible fluids in contact with each other through an interface. This interface takes place on the upper dew-point and the bubble-point curves. The magnitude of IFT depends on the saturation curve under study.

Investigating the magnitude of IFTs in oil- and gas-dominated systems for a mixture containing methane–hexane (70–30 %) showed notable variances as shown in Fig. 11. This mixture was selected to justify the variant IFT impact on reservoir performances in reference to the work of Nojabaei et al. (2013). Examining the influence of IFT indicated an increase in the upper dew-point pressure and a decrease in the bubble-point pressure. IFT values were investigated to the right and left of the critical point as illustrated in Fig. 11. The results indicated zero IFTs around the critical point, indicating no interface between the phases. The values of IFT as the temperature extends toward the oil-dominant system at lower temperatures expand largely due to the increase in liquid density. The increase in IFT values leads to decreasing the bubble-point pressure indicating more domination of the oil phase, and delay of the gas phase appearance. In contrast, the changes in IFT toward higher temperatures in the gas-dominant system show limited effect compared to those found in the oil side. The outcome of this exercise advocates lower impact of capillary pressure on the performance of gas reservoirs in comparison with oil reservoirs. Furthermore, an investigation on the sensitivity of nanopore sizes to the behavior of IFTs according to temperature was carried out. Three nanopore sizes were used: 20, 10, and 5 nm. The overall behavior of IFTs at temperatures ranging from 100° F to 320° F showed little influence on the values of IFTs.

Figure 12 presents an IFT ratio of oil-to-gas-dominated systems for methane–hexane (70–30 %) obtained at different pore throat sizes. In all of the cases, the IFT values for the oil-dominated system are fixed. As the pore throat sizes become smaller, the IFT values in the gas system decrease, causing the IFT ratio to increase. The decrease in IFT values in the gas-dominated system becomes vivid at lower temperatures, which approaches zero as the temperature descends toward the critical point. It can be seen that IFT ratios become very low at higher temperatures indicating higher IFT values in the gas region. However, reservoirs with temperatures closer to the cricondentherm contain less condensate and fall under the classification of wet-gas

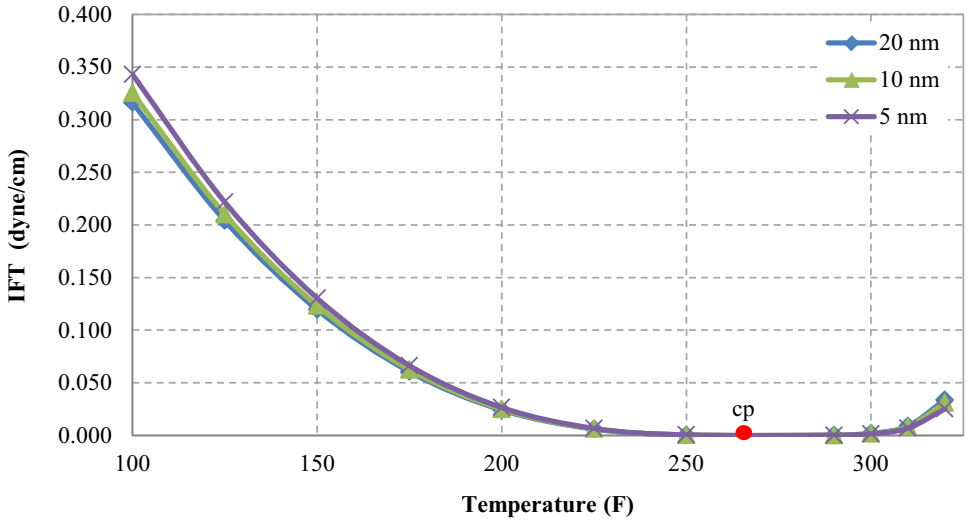

Fig. 11 IFT values at different temperatures for methane–hexane (70–30 %)

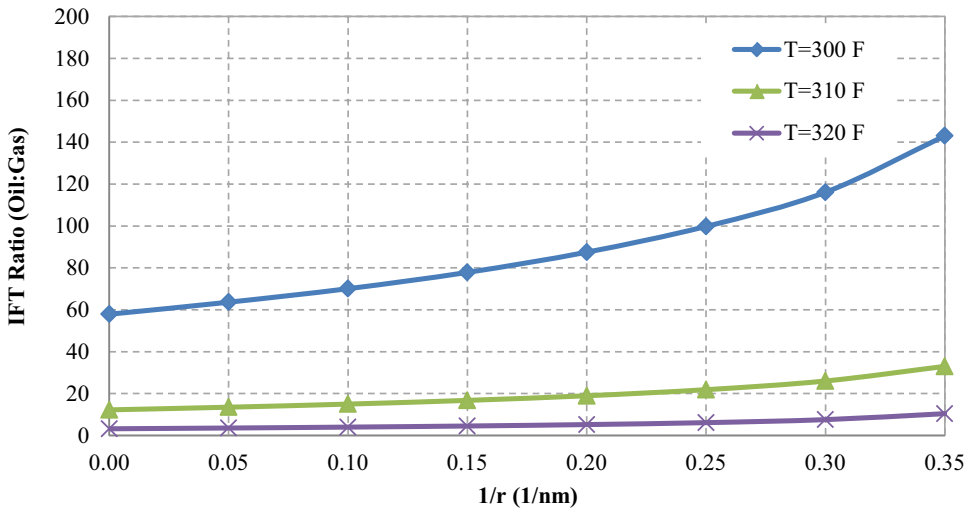

Fig. 12 IFT ratio of oil–gas-dominated systems for methane–hexane (70–30 %)

reservoirs. IFT ratios indicate that at the minimum impact of pore throat sizes to increase capillary pressure, IFT in the oil side can be as high as 140 times the IFT values in the gas side. At lower temperatures closer to the critical point, IFT in the oil can reach up to 500 times the gas IFT values. In summary, Figs. 11 and 12 suggest that IFT values are more significant in oil-dominated reservoirs than in gas reservoirs. As a result, the influence of IFT on the performance of liquid-rich gas reservoirs was less evident.

Performance while activating diffusion and capillary forces

Diffusion was first introduced by Fick in 1855 to capture flow resulting from the exchange of matters through porous media. In 1986, Ertekin et al. introduced the concept of multi-mechanistic domains, where the fluids flow as a function of pressure and concentration gradients, thus allowing the gas to flow as per Darcy's law in pressure domains, and flow by diffusion under Fick's law when conductivity becomes an issue. This work continues to evaluate flow performance of unconventional phenomena in liquid-rich gas reservoirs such as the inclusion of diffusion while activating capillary forces.

The activation of capillary pressure showed relative increase in the thickness of condensate during the first 40 days of production prior to invading the majority of the blocks. Subsequently, this imposed resistance for gas to flow and increased residence time of condensate. Thus, it is important to appraise flow behavior and contribution of the matrix to production knowing that diffusion will enhance recovery. Generally, diffusion improved the depletion behavior in nanopores, as shown in condensate evolution and recovery profiles. Figure 13 shows that the system containing the mixture methane–hexane with concentration

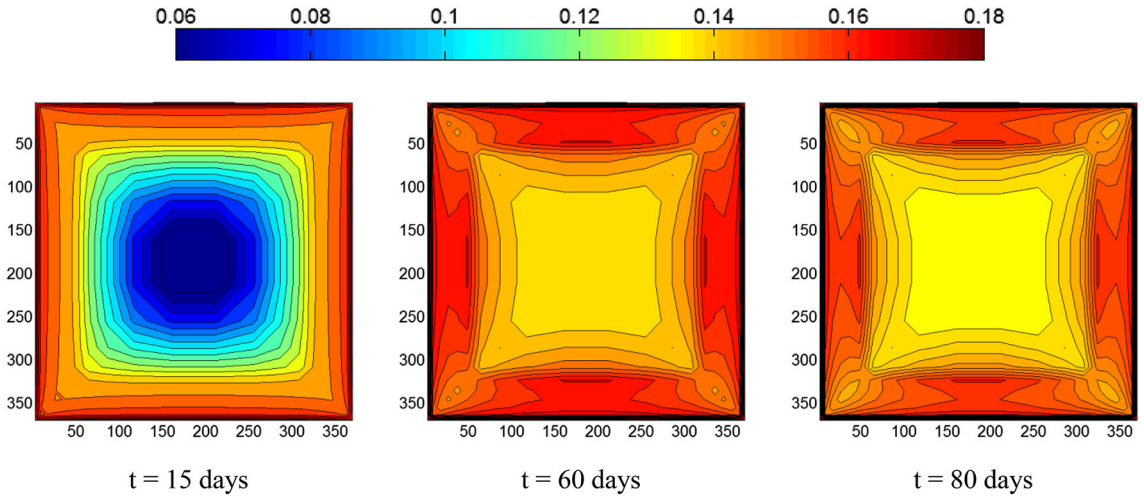

Fig. 13 Condensate evolution for methane–hexane (85–15 %) with the inclusion of capillary forces ($r = 10$ nm) and diffusion (10 ft^2/day)

of 85 and 15 % is subjected to higher depletion with the inclusion of diffusion. It indicates rapid fluid movement toward the fractures while activating capillary forces using a pore throat radius of 10 nm. The saturation profile at the corners and sides of the matrix experiences higher evolution than the center of the block due to the enhancement in condensate evolution. Similar to the rest of the studied cases, diffusion advances the evolution of condensate at the neighboring blocks to the fractures. This capability had reduced the resistance applied on the stored gas at the inner part of the matrix from flowing toward the flow channels. The outcome suggests extensive influence of diffusion even with the inclusion of capillary forces that by 30 days all of the blocks have been flushed with condensate. It also shows expedited condensate evaluation with diffusion, where re-vaporization of condensate has been reached before 60 days of simulation. The re-vaporization is shown by the reduced saturation at the corners of the grid block illustrated in Fig. 13.

Figures 14 and 15 display the gas and condensate recovery obtained from the numerical study using the compositional combinations that presented the highest condensate at reservoir conditions. The gas recovery of the moderate fluid came to be the highest because of diffusion domination. Since the mixture methane–hexane (85–15 %) reflected higher reservoir condensation, it indicates severe impairment to the gas flow under pressure gradient. Once diffusion was activated, flowing under concentration gradient became a prominent factor leading to additional gas extractions. Gas recovery for the moderate, light, and heavy mixtures with diffusion was determined to be 49.48, 45.98, and 43.17 %, respectively. Activating diffusion allows more gas to flow freely to the surface containing higher content of heavy concentrations, which under surface conditions yields higher condensate dropouts. Figure 15 displays the condensate recovery for the same mixtures above. Methane–decane produced higher condensate recovery than the moderate mixture because it is the least volatile mixture.

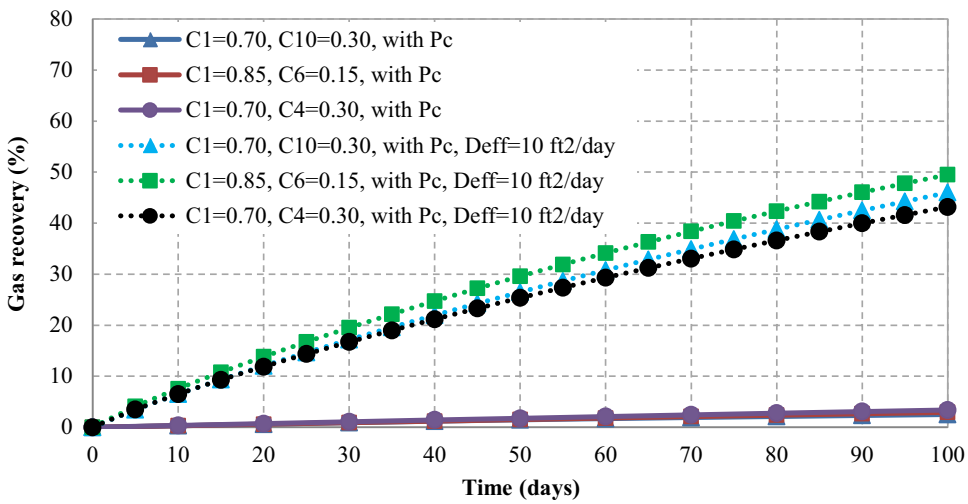

Fig. 14 Gas recovery improvement with diffusion

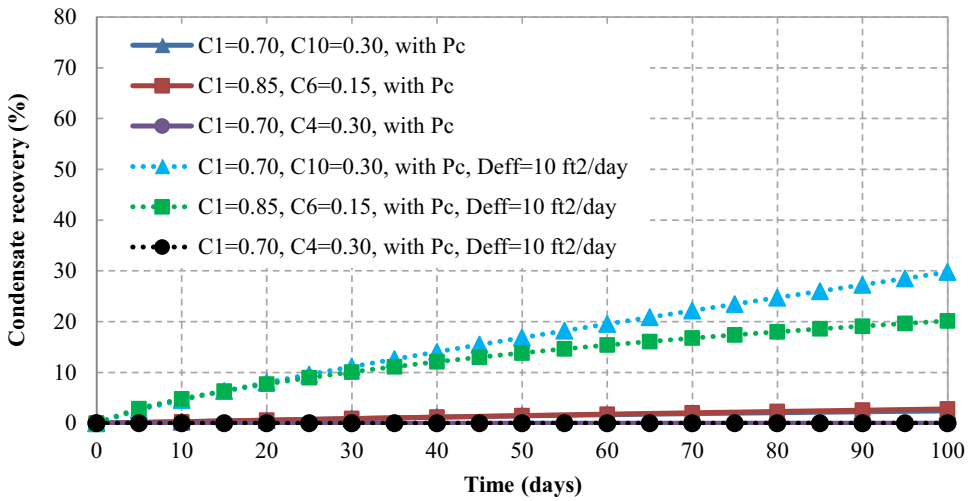

Fig. 15 Condensate recovery improvement with diffusion

The heavy and moderate mixtures turned in condensate recovery of 29.76 % and 20.15 %, while methane–butane continued to show the least amount of condensate at surface conditions. The recovery of liquid-rich gas in tight formations was improved with the activation of the multi-mechanistic flow to account for additional extractions that are able to flow in the concentration gradient domain.

Concluding remarks

Several sets of composition combinations had been used for the analysis of capillary pressure's effect on dew point in nanopores. The relationships developed showed an increase in capillary pressure with smaller pore throat sizes for the upper dew-point pressure. Evidently, higher changes in interfacial tensions were associated with higher capillary forces. Capillary forces' magnitudes depended on composition combinations and concentrations. Among the three combinations for light, moderate, and heavy mixtures, methane–hexane and methane–butane delivered the highest capillary pressures with concentration of 85 and 15 %, whereas the rest of the mixtures including those with concentrations of 60 % volatile and 40 % non-volatile recorded the least capillary pressure.

The influence of capillary forces on the flow behavior of liquid-rich gas reservoirs was explored to assess flow resistance, condensate evolution, and performance. The outcome indicated minuscule effects of capillary forces on reservoir pressure, oil saturation, and productivity. Magnifying the influence of capillary forces using methane–hexane (85–15 %) with 10-nm pore throat radius showed enhanced condensate spread. Condensate had invaded 44 % of the blocks in comparison to 23 % without activating capillary pressure after 40 days. Once condensate reached the inner portion of the block, the spread evolution becomes negligible. Furthermore, the capillary forces employed limited retention on productivity. The smallest pore throat radius recorded a decrease in recoveries by a magnitude of less than 1 %. Thus, diminutive influences were witnessed to increase the residence time of condensate and impose resistance to impact productivity.

The insignificance of the inclusion of capillary pressure on the performance of liquid-rich gas reservoirs in contrast to oil reservoirs was found to be highly dependent on IFT values. Investigating IFT values from an oil-dominated system against IFT values from a gas-dominated system showed significant variances. Interfacial tensions recorded the lowest values in a gas-dominated system and the highest in an oil-dominated system. This was due to having lower density differences in the gas side than in the oil side of the phase envelope. The magnitude of IFTs in the oil side suggested more significance in the oil-dominated reservoirs than in gas reservoirs.

Depletion behavior associated with activating diffusion enhanced condensation evolution and recoveries for all the mixtures. Diffusion reduced the resistance applied against the flow of gas toward the flow channels, which excessively enhanced the depletion behavior. In addition, larger withdrawal was witnessed for both phases due to the domination of the diffusion mechanism over Darcy's law. Gas recoveries for all the mixtures reflected notable increases because of diffusion domination. Mixture with the least volatile concentrations recorded higher condensate recoveries. The improved performance is owed to the activation of the multi-mechanistic flow to account for additional recoveries that are unable to be extracted under the Darcy's law pressure gradient.

The variation of reservoir fluid distribution can be caused by many factors: production scheme, diffusion gradient, permeability, wettability conditions, and relative permeability. It is highly recommended for future work to apply different matrix conditions that might magnify the effect of capillary forces on the distribution of fluids. Areas

for further investigation include: capturing effect of multi-mechanistic flow in the liquid phase, mapping the dominant effect of diffusion over capillary pressure against different wettability conditions and permeability constraints, and investigating the sensitivity of the coupled PBM–capillary model by experimental validation using methane–butane (85–15 %) at 100 °F.

Acknowledgments I would like to thank Saudi Aramco for their sponsorship and continuous support which have contributed vastly to my development and success. My gratitude is due to Dr. Luis Ayala, for his unlimited support, guidance, and valuable friendship.

Appendix 1: Data

See Tables 1 and 2.

Table 1 The variables used for the simulation scenarios

Matrix		
Matrix block dimension (single)	372	ft
Grid blocks of system (single)	22 × 22 × 1	blocks
Matrix block dimension (quarter)	186	ft
Grid blocks of system (quarter)	11 × 11 × 1	blocks
Reservoir pressure	3–4 % above Pdew	
Pore throat radius	1×10^{12}, 10, 20	nm
Rock compressibility	0	cp^{-1}
Porosity	0.13	
Permeability	0.1	mD
Effective diffusion	0 and 10	ft^2/day
Fracture		
Fracture pressure	500	psia
Fracture width	0.01	ft
Fracture permeability	2000	mD

Table 2 Properties of the phases presented in the system

Relative permeability	
Water saturation (swirr)	0.16
Critical oil saturation	0.28
Oil/gas	SPE third comparative
Oil/water	Solution project

Appendix 2: Numerical simulator

Numerical reservoir simulation is a modeling technique greatly used in the development, forecasting, and prediction of productivity of reservoirs to obtain higher recoveries. A fully implicit compositional simulator was developed according to the formulations presented in Eq. (24), to simulate the productivity of liquid-rich gas reservoirs in tight formations.

$$\nabla \cdot \left[x_i \bar{\rho}_o \vec{v}_{io} + y_i \bar{\rho}_g \vec{v}_{ig}\right] + \frac{F_i}{V_b} = \frac{\partial}{\partial t}\left[\phi\left(x_i \bar{\rho}_o S_o + y_i \bar{\rho}_g S_g\right)\right], \quad i = 1, 2, \ldots, n_c \tag{24}$$

A suitable velocity model was substituted in the molar velocity terms of Eq. (24) to represent the flow of fluids within the system. The model used for this work was built to accommodate fluids flowing under Darcian law in pressure domains and under Fick's law in concentration domains. Using Darcy's law, the flow of fluid depends on permeability, viscosity, and the pressure gradient. Flowing under Fick's law, the flow becomes function of the diffusion coefficient and density gradient. In return, the total velocity of gas and condensate is a result of the flow driven by the bulk Darcian effect ($\vec{v}_{if}^{D}$) and Fickian effect ($\vec{v}_{if}^{F}$). However, since the diffusion effect represented by Fick's law for the liquid phase is a hundred times less effective than in the gas phase, the diffusion term for the liquid phase is abandoned (Ayala 2004). Equations (25) and (26) represent the total molar velocity of gas and condensate.

$$\vec{v}_{io} = \vec{v}_o^{D} = -5.615 \frac{k k_{ro}}{\mu_o} \nabla \Phi_o \tag{25}$$

$$\vec{v}_{ig} = \vec{v}_g^{D} + \vec{v}_{ig}^{F} = -5.615 \frac{k k_{rg}}{\mu_g} \nabla \Phi_g - \phi S_g \frac{D_{eff}}{\rho_g} \nabla \bar{\rho}_g \tag{26}$$

In order to attain a numerical solution, the flow equations are discretized using algebraic approximation of the second-order derivatives with respect to space and first-order derivatives with respect to time. The developed algebraic equations remain nonlinear and require further treatment. Solving the flow equation requires using a linearization method, and one of the commonly used linearization methods is the Newton–Raphson. The developed in-house simulator utilizes Newton–Raphson iterative method with fully implicit type equations to solve for the unknowns at the same times step.

References

Abaa K, Wang JY, Ityokumbul MT (2012) Parametric study of fracture treatment parameters for ultra-tight gas reservoirs. SPE paper 152877 presented at the Americas Unconventional

Resources Conference held in Pittsburgh, Pennsylvania, USA, 5–7 June. doi:10.2118/152877-MS

Ahmed TH (2000) Reservoir engineering handbook, 2nd edn. Gulf Professional Publishing Co. ISBN 0-88415-770-9

Al Ghamdi BN (2009) Analysis of capillary pressure and relative permeability effects on the productivity of naturally fractured gas-condensate reservoirs. M.Sc. thesis. The Pennsylvania State U., University Park, Pennsylvania

Ayala LF (2004) Compositional modeling of naturally-fractured gas-condensate reservoirs in multi-mechanistic flow domains. PhD dissertation. The Pennsylvania State University

Ayala LF, Ertekin T, Adewumi M (2004) Analysis of recovery mechanisms for naturally fractured gas-condensate reservoirs. SPE paper 90010 presented at the SPE Annual Technical Conference and Exhibition held in Houston, TX, 26–29 Sept. doi:10.2118/90010-MS

Ayala LF, Ertekin T, Adewumi M (2006) Compositional modeling of naturally-fractured gas-condensate reservoirs in multi-mechanistic flow domains. SPE J 11(04):480–487. doi:10.2118/94856-PA.SPE-94856-PA

Ayala LF, Ertekin T, Adewumi M (2007) Numerical analysis of multi-mechanistic flow effects in naturally fractured gas-condensate systems. J Pet Sci Eng 58(01):13–29. doi:10.2118/107870-PA.SPE-107870-PA

Ayyalasomayajula P, Silpngarmlers L, Berroteran J, Sheffield J, Kamath J (2003) Measurement of relevant gas condensate relative permeability data for well deliverability predictions for a deep marine sandstone reservoir. Paper SCA2003-33 presented at the 2003 SCA international symposium, Pau, France, 22–25 Sept

Ellis CP (1932) Ethyl palmitate. Its density, surface tension, parachor, and Eötvös–Ramsay–Shields coefficient. J Chem Soc 1697–1699. doi:10.1039/JR9320001697

Ertekin T, King GA, Schwerer FC (1986) Dynamic gas slippage: a unique dual-mechanism approach to the flow of gas in tight formations. SPE formation evaluation, pp 43–52. doi:10.2118/12045-PA.SPE-12045-PA

Fick A (1855) Über diffusion. Ann Phys 170(1):59–86

Holditch SA (2006) Tight gas sands. J Petrol Technol 58(06):86–93. doi:10.2118/103356-JPT.SPE-103356-JPT

Macleod DB (1923) On a relation between surface tension and density. Trans Faraday Soc 19:38–41. doi:10.1039/TF9231900038

Michelsen M (1982) The isothermal flash problem. Part I. Stability. Fluid Phase Equilibria 9(1):1–19. doi:10.1016/0378-3812(82)85001-2

Nojabaei B, Johns TR, Chu L (2013) Effect of capillary pressure on phase behavior in tight rocks and shales. SPE Reservoir Eval Eng 16(03):281–289. doi:10.2118/159258-PA.SPE-159258-PA

Nojabaei B, Siripatrachai N, Johns TR, Ertekin T (2014) Effect of saturation dependent capillary pressure on production in tight rocks and shales: a compositionally-extended black oil formulation. SPE paper 1171028 presented at the SPE Eastern Regional Meeting held in Charleston, WV, USA, 21–23 Oct. doi:10.2118/171028-MS

Phillip C, Etherington JR, Aguilera R (2010) A process to evaluate unconventional resources. SPE paper 134602 presented at the SPE annual technical conference and exhibition held in Florence, Italy, 19–22 Sept. doi:10.2118/134602-MS

Ramsay W, Shields J (1893) Phys Z Chem Leipz 12:433

Sugden S (1924) The variation of surface tension with temperature and some related functions. J Chem Soc 125:32–41. doi:10.1039/CT9242500032

Van der Waals JD (1910) The equation of state for gases and liquids. Nobel lectures in Physics 1901-1921, pp 254–265

Warren JE, Root PJ (1963) The behavior of naturally fractured reservoirs. SPE J 3(03):245–255. doi:10.2118/426-PA.SPE-426-PA

Weinaug CF, Katz DL (1943) Surface tension of methane-propane mixtures. Ind Eng Chem 35(2):239–246. doi:10.1021/ie50398a028